The MAP4 Projection Domain Accelerates Hypoxia-Induced Mitophagy Disruption through LIR Motif in Cardiomyocytes

Yuesheng Huang (yshuangtmmu@163.com)
Institute of Burn Research, Southwest Hospital, Third Military Medical University (Army Medical University)

Yanhai Feng
Third Military Medical University

Qiong Zhang
Third Military Medical University

Lingfei Li
Third Military Medical University

Junhui Zhang
Third Military Medical University

Yao Huang
Third Military Medical University

Yanling Lv
Third Military Medical University

Jiezhi Jia
Third Military Medical University

Dongxia Zhang
Third Military Medical University

Gaoxing Luo
Third Military Medical University

Jiongyu Hu
Third Military Medical University

Article

Keywords: cardiomyocyte, cardiac dysfunction, mitophagy, hypoxia, MAP4 PJ

Posted Date: November 15th, 2021

DOI: https://doi.org/10.21203/rs.3.rs-1014224/v1

Abstract

Previously, we and other investigators have demonstrated that phosphorylated microtubule-associated protein 4 (p-MAP4) impacts myocardial hypertrophy and ischemic heart failure. However, the detailed mechanism behind this remains under elucidated. Published studies have suggested that impaired mitophagy contributes to hypoxia-induced myocardial damage, hence the involvement of p-MAP4 in mitophagy in cardiomyocytes was investigated. The results herein revealed that there was increased degradation of mitochondria, accumulated mitophagosomes and disrupted autophagic flux in both neonatal and adult ones of *MAP4*-knockin (KI) mice. This indicated that p-MAP4 persistently degraded mitochondria through activating mitophagy. Next, Tom70 was found as the importer of p-MAP4 in the context of mitochondrial translocation. And, the LC3-interacting region (LIR) motif (47–50aa) caused p-MAP4-induced mitochondrial engulfment, and the ubiquitin-interacting motif (UIM) domain determined the characteristics of p-MAP4-induced mitophagosomes, which were structure and membrane potential-independent. Moreover, p-MAP4 enhanced hypoxia-induced mitophagic flux impairment, and p-MAP4 LIR (47–50aa) mutation decreased hypoxia-induced autophagy both in *MAP4* knockout and wildtype cardiomyocytes. Overall, this study identified that p-MAP4 as a novel mediator and cargo receptor in mitophagy, and that the degradation of the MAP4 PJ domain as a promising therapeutic target for improving the cardiac function of hypoxia-related heart failure or cardiac remodelling.

Introduction

Mitophagy, an essential part of selective autophagy, is a highly regulated process involved in the degradation of damaged or redundant mitochondria[1]. To date, two mitophagy mechanisms have been proposed. One depends on PTEN-inducible putative kinase 1 (Pink1)-Parkin pathway for the ubiquitination of mitochondrial proteins followed by interactions with the adaptor protein p62 (SQSTM1), which is responsible for connecting ubiquitin with LC3 (a marker of phagophores)[2]. The other mechanism relies upon either proteins or lipids on the outer mitochondrial membrane as receptors for LC3. NIP3-like protein X (Nix/Bcl-2L), Bcl-2, and FUN14 domain containing 1 (FUNDC1) have been shown to act as LC3 receptors and are known as LC3-binding proteins[3–5]. The LIR and the UIM have been regarded as the functional domains in the LC3-binding proteins, which underly binding to the LC3 LIR/AIM docking site (LDS) or UIM/AIM docking site (UDS)[6–7]. LIR is a short linear motif that consists of up to 13 amino acids with a W/F/Y-XX-L/I/V core sequence (where X indicates sites that can be replaced by any amino acid)[7]. The UIM domain consists of 20 amino acids with a principal sequence of XXXXX-L-XX-A-XXX-S-XXXXXXX, which is associated with the induction of ubiquitination and binding to ubiquitinated proteins[8]. In mitophagy, the interaction between LIR or UIM-containing proteins and LC3 is the core step, which promotes the engulfment of mitochondria by autophagosomes. Importantly, Huang et al [9] proposed that mitophagy played a role in the regulation of heart function in a myocardial ischemia-reperfusion model. Therefore, a complete understanding of mitophagy in the context of cardiac hypoxia, as well as the associated regulatory mechanisms, is essential for the development of new therapeutic interventions to treat hypoxia-induced heart dysfunction.

Microtubules (MTs) are thought to participate in autophagy processes, including the formation of autophagosomes and their fusion with lysosomes[10, 11]. Microtubule-associated proteins (MAPs) are cytosolic skeleton proteins that are important for the polymerisation of MTs[12]. MAP4 is among the most extensively studied MAPs, and it is ubiquitously expressed in non-neural cells and becomes functional upon phosphorylation (p-MAP4)[12–14]. MAP4 consists of a N-terminal projection (PJ) domain and a C-terminal MT-binding (MTB) domain[15]. The PJ domain is further subdivided into three distinct regions, the Na-region (the N-terminal 247 amino acid residues), the KDM-region (344 amino acid residues from 248 to 592) and the b-region (94 amino acid residues from 593 to 687)[15]. The MTB domain is also divided into the proline-rich region (Pro-rich), the assembly promoting-repeated (AP) sequence region and the hydrophobic tail region[16]. To date, studies on MAP4 have mainly focused on the MTB domain, which can be phosphorylated (at S667, S737, and S760) and leads to MT depolymerisation, myocardial apoptosis and myocardial hypertrophy[13, 17, 18]. It is noteworthy that p-MAP4 (at the MTB domain) was shown to translocate into the outer mitochondrial membrane leading to mitochondrial injury and the initiation of apoptosis[18]. However, its effects on mitophagy and the function of the PJ domain remain obscure.

Heart failure is associated with a high mortality rate (50% for 5 years) no matter whether it is induced by pathological cardiac remodelling, hypoxia, ischemic-reperfusion injury or other diseases[17]. Previous investigations, by both others and ourselves, have demonstrated that p-MAP4 caused myocardial hypertrophy and ischemic heart failure[17, 19]. However, the mechanisms underlying the incidence of hypoxia induced heart failure requires further investigation. Recent data has highlighted mitophagy as one of the principal mediators of heart function under several pathological conditions, including hypoxia and myocardial ischemia-reperfusion injury[9]. Moreover, p-MAP4 was recently shown to translocate into mitochondria in cardiomyocytes under hypoxic conditions[18]. Thus, to determine the possible mechanisms of p-MAP4 induced myocardial damage, the effects of p-MAP4 on mitophagy in cardiomyocytes were investigated herein.

Results

Increased p-MAP4 degrades mitochondria through impacting mitophagy in the whole life of mice

MAP4-knock in (KI) mice were used to determine the effects of MAP4 phosphorylation on mitophagy in the context of normoxia, the protocol for the generation of these mice has previously been described [17]. As shown in Fig. 1A, increased phosphorylation of MAP4 was observed at residues S737 and S760 in the myocardium of *MAP4*-KI mice (P=<0.05). Next, the mitochondrial proteins (TOM20, VDAC1 and TIM23) were significantly decreased in the myocardium of *MAP4* KI mice, but the endoplasmic reticulum (calnexin) and Golgi marker (GM130) were not changed (Fig. 1B, P=<0.05). Meanwhile, elevated expressions of LC3II, Atg3, Atg7, Beclin1, Bcl-2, and P62 were observed in the myocardium of *MAP4*-KI

mice, which correlated with an increased number of mitophagosomes (Fig. 1C and 1D, p<0.05). These results demonstrated that p-MAP4 degraded mitochondria and activated mitophagy in adult mice.

Next, to investigate the effects of p-MAP4 on mitophagy in neonatal mice, the primary cardiomyocytes of neonatal *MAP4* KI mice were isolated. Importantly, similar significant expressions increases were observed for autophagy-related proteins in the isolated primary cardiomyocytes of *MAP4* KI mice (Fig. 1E, P=<0.05). Furthermore, increased mitophagy activation (with GFP-LC3 and Dsred-Mito signals) and more mitophagosomes using TEM (Transmission Electron Microscopy) were observed. Slightly disrupted autophagic flux (based upon mRFP-GFP-LC3 signals) was also observed (Fig. 1F-J, P=<0.01). Together, these results indicated that p-MAP4 degraded mitochondria by impacting mitophagy both in neonatal and adult mice under normoxia, hinting the influences of p-MAP4 on mitophagy in cardiomyocytes were persistent.

Tom70 Mediates The Mitochondrial Translocation Of P-map4

The mitochondrial translocation of p-MAP4 has previously been reported to be the first step of mitophagy initiation[18]. To determine the mechanism behind the mitochondrial translocation of p-MAP4, a qualitative (shotgun) protein analysis was used to detect MAP4-interacting proteins in primary cardiomyocytes. This analysis revealed that *Tomm70*/Tom70 and *Hspd1*/HSP60 were the potential importers of MAP4 into the mitochondria (Fig. 2A). As demonstrated in Fig. 2B, Ad-MAP4 (Glu) cardiomyocytes effectively increased the levels of p-MAP4 (at both the S737 and S760 residues; P=<0.05). Importantly, the expressions of HSP60 and Tom70 were increased in cardiomyocytes overexpressing MAP4 (Glu) or those subjected to hypoxia (Fig. 2C). Moreover, specific siRNAs targeting Tom70 and HSP60 were constructed that efficiently knocked down their expressions (Fig. 2D). As shown in Fig. 2E-F, Tom70 siRNA significantly decreased Ad-MAP4 (Glu) and hypoxia-induced high LC3II expression in extracted mitochondrial proteins. Importantly, knocking down Tom70 decreased the co-localisation of p-MAP4 with the mitochondria and mitophagosomes (Fig. 2G-J, P=<0.05). Together, these results demonstrated that p-MAP4 translocation to the mitochondria (and thereby mitophagy activation) was Tom70 dependent.

The LIR (47–50aa) in MAP4 determines mitochondrial engulfment and degradation

Substrate recognition was then explored to further clarify the mechanism of mitochondrial engulfment induced by p-MAP4, during which LC3 was concentrated for it was a major regulator of substrate recognition during mitophagy[6]. As shown in Figures 3A, 3B, S1C and S1D, MAP4 co-localised and interacted with LC3; importantly this was weakened in the context of Bcl-2 knockdown. This data suggested that the MAP4/LC3 complex was formed after the translocation of p-MAP4 into the mitochondria. Based upon this observation, potential LIRs (34–37aa and 47–50aa) and a UIM (463–482aa) were sought and found in MAP4 (Fig. 3C and 3D). These two motifs are also within the MAP4 PJ domain (Fig. 3E). The use of targeted point-mutated MAP4 (Ala) confirmed that the MAP4/LC3

interaction was phosphorylation-dependent (Fig. 3F). Additionally, selective exogenous expression the wild type or mutant MAP4 PJ domain was conducted for *in vitro* binding assays using GST-tagged LC3. This analysis indicated that MAP4 LIR truncation, not UIM truncation, impacted the direct interaction of MAP4 with LC3 (Fig. 3G and Fig. 3H). Considering two LIRs were contained in MAP4-1, *MAP4-1 LIR*$^{\triangle 34,37}$ and *MAP4-1 LIR*$^{\triangle 47,50}$ were then constructed, which facilitated the observation that *MAP4 LIR (47–50aa)* was the core LIR responsible for MAP4/LC3 interaction (Fig. 3I and 3J). Furthermore, the LIR $^{(47,50)}$ -mutant MAP4 (Glu) effectively downregulated Ad-MAP4 (Glu) induced autophagy activation in primary cardiomyocytes, whereas LIR $^{(34,37)}$ -mutant MAP4 (Glu) had no such effect (Fig. 3K). And, LIR $^{(47,50)}$ -mutant MAP4 (Glu) reversed MAP4 (Glu) induced mitochondrial proteins (VDAC1, Tom20 and TIM23) degradation (Fig. 3L). These results indicated that MAP4 LIR (47-50aa) was responsible for p-MAP4 induced mitochondrial engulfment and degradation.

The UIM domain maintains the specific characteristics of p-MAP4 induced mitophagy

Firstly, LC3 was found to co-localised in linear mitochondria in Ad-MAP4 (Glu)-transduced or hypoxia treated cardiomyocytes, but not in Carbonyl cyanide 4-(trifluoromethoxy)phenylhydrazone (FCCP)-treated ones (Fig. 4A). Notably, the number of such mitophagosomes was highest in cardiomyocytes treated by Ad-MAP4 (Glu) (Fig. 4C). Moreover, the engulfed mitochondria showed high membrane potential in Ad-MAP4 (Glu)- or hypoxia-treated cardiomyocytes, but not in FCCP-treated ones (Fig. 4B). Again, the proportion of engulfed mitochondria with high membrane potential was highest in Ad-MAP4 (Glu) treated cardiomyocytes when compared to the hypoxia or FCCP treated ones (Fig. 4D). These results indicated that p-MAP4-induced mitophagy was neither structurally nor potential-dependent.

Further studies were conducted focusing upon the MAP4 UIM domain because ubiquitination has emerged as a universal cargo recognition signal, although it appears irrelevant to mitochondrial function[22]. It's noteworthy that the level of ubiquitination was increased under normoxia in the myocardium, primary cardiomyocytes and mitochondrial membrane of *MAP4* KI mice (Fig. 4E and S1F). To verify the function of the MAP4 UIM domain, the mutual effects of MAP4 and ubiquitin were explained, and determined to be increased in Ad-MAP4 (Glu)-treated cardiomyocytes (Fig. 4F). Importantly, UIM mutant-MAP4 (Glu) decreased the co-localisation of GFP-LC3 with TMRE (Tetramethylrhodamine ethyl ester) (Fig. 4G-H, P=<0.001). In fact, general mitophagosomes (as opposed to structural and potential-independent mitophagosomes) were observed in cells incubated with UIM mutant-MAP4 (Glu) (Fig. 4I-J). Furthermore, Ad-MAP4 (PJ) induced stronger cytotoxicity than UIM mutant-MAP4 (Glu) (Fig. 5K, P=<0.01). Together, these results indicated that the MAP4 UIM domain was essential for p-MAP4-induced non-structural and non-potential-dependent mitophagosomes.

The MAP4 LIR (47–50aa) determinates p-MAP4 increased autophagy under hypoxic conditions

Next, the effects of increased p-MAP4 on mitophagy under hypoxic conditions were examined. Primary cardiomyocytes were pre-treated with Ad-MAP4 (Glu) for 48 hours prior to hypoxia exposure. And, both Ad-MAP4 (Glu)-treated cardiomyocytes and primary cardiomyocytes from *MAP4*-KI mice were used as

effective p-MAP4 models. Importantly, increased p-MAP4 amplified the levels of autophagy-related proteins (LC3II, Atg3, Atg7, Atg16L1, Beclin1, Bcl-2 and P62) under hypoxic conditions (Fig. 5A and 5B, P=<0.05). Furthermore, increased mitophagosomes, mitophagy and autophagy flux impairments were observed in cardiomyocytes overexpressing p-MAP4 (both models) under hypoxia versus that seen in the control cardiomyocytes (Fig. 5C-G, P=<0.01). These results indicated that p-MAP4 underlain mitophagy activation and impairment in response to hypoxia *in vitro*.

Then, the effects of p-MAP4 on hypoxia induced mitophagy *in vivo* in adult *MAP4*-KI mice were further investigated. As shown in Fig. 5H, there were higher expressions (P=<0.05) of LC3-II, Atg3, Atg7, Atg16L1, Beclin1, Bcl-2 and p62 in the myocardium of *MAP4*-KI mice after expose to hypoxia (when compared to wild-type mice), which was also associated with more mitophagosomes (Fig. 5I). These results were in line with the *in vitro* data.

Next, the influences of p-MAP4 inhibition on hypoxia induced autophagy were investigated. As a complementary approach, MARK4 was silenced in cardiomyocytes using specific siRNAs, because it has been identified as an upstream regulator of p-MAP4[19]. As shown in Fig. 5K, MARK4 was effectively silenced and the reduction of its expression led to a decline in the overexpressed LC3-II in cardiomyocytes under hypoxia *in vitro*. These data indicated p-MAP4 inhibition decreased hypoxia activated autophagy.

Furthermore, to identify the effects of LIR (47-50aa) and BH3 domains on hypoxia induced autophagy, Ad-LIR $^{(47,50)}$ -mutant MAP4 (Glu) and Ad-BH3-mutant MAP4 (Glu) were used. In hypoxic cardiomyocytes, Ad-LIR $^{(47,50)}$ -mutant MAP4 (Glu), rather than Ad-BH3-mutant MAP4 (Glu), reduced hypoxia induced autophagy (Fig. 5L). In hypoxic cardiomyocytes pre-treated with MAP4 siRNA, the Ad-LIR $^{(47,50)}$ -mutant MAP4 (Glu) reduced the p-MAP4-enhanced LC3 II in hypoxic cardiomyocytes; whereas Ad-BH3-mutant MAP4 (Glu) displayed no effect (Fig. 5M). Together, these results demonstrated that the MAP4 LIR (47–50aa) determined p-MAP4 increased autophagy activated by hypoxia.

Discussion

Mitochondrial dysfunction is a crucial contributor to myocardial injury. Previous research revealed that p-MAP4 caused myocardial hypertrophy and ischemic heart failure, which was dependent upon mitochondrial dysfunction[17, 19]. Autophagy, including mitophagy and neutrophil autophagy, is essential for the degradation of disrupted mitochondria and is consequently important for the regulation of myocardial function[23–25]. We have previously reported that p-MAP4 translocated to mitochondria in hypoxic cardiomyocytes[18]; however, the role of p-MAP4 on mitophagy in cardiomyocyte had not previously been explored. Herein, p-MAP4 was demonstrated to mediate mitochondrial engulfment through its LIR (47-50aa), and maintain structure- and voltage-independent characteristics through its UIM domain. This study highlights MAP4 not only as a new LIR and UIM domain-containing protein, but also as a novel autophagic cargo acceptor. It is noteworthy that these domains predominantly locate within the MAP4 PJ domain and are activated by phosphorylation of the MTB domain. This discovery indicates that the PJ domain is responsible for the core functionality of MAP4 in mitophagy. Moreover, p-

MAP4 suppresses the disruption of mitophagic flux induced by hypoxia. Overall, this article identified MAP4 as another novel cargo receptor and that the degradation of MAP4 PJ domain is a promising therapeutic target to improve the cardiac dysfunction of hypoxia-related cardiac remodelling or heart failure.

The N-terminus has been reported to be the functional region for the vast majority of molecules [26]. Therefore, the role that the PJ domain (which is in the N-terminal region of MAP4) was determined to play in this study is not unprecedented. Moreover, three new domains within the MAP4 PJ domain were also described, namely: the BH3, LIR and UIM domains. The importance of the PJ domain is also supported by the findings by Junko et al [15], which revealed that the PJ domain represses the microtubule-bundling activity of the MTB domain. In the present study, the PJ domain was shown to strongly interact with both LC3 and Bcl-2 (Fig. 3). Together, this data strongly supports the hypothesis that the PJ domain is arguably the most biologically important MAP4 domain. It is notable that the phosphorylation of the MTB domain underlies the MAP4/LC3 and MAP4/Bcl-2 interactions (Fig. 3 and 4). Several post-translational modifications have been reported as the stimulating factors underpinning the biological functions of proteins. For example, LC3/Bnip3L or LC3/Fundc1 interactions were also reported to be phosphorylation-dependent[27], and Mariya et al [26] demonstrated that the O-GlcNAcylation of histone deacetylase 4 activated its N-terminus and was associated with cardiac protection in diabetes models. It is possible that the MTB and PJ domains reciprocally regulate each other via acylating modifications. Under physiological conditions, MAP4 mainly shows microtubule-binding activity through its MTB domain, whereas the PJ domain is inactivated. Whereas under pathological conditions, MTB domain phosphorylation activates the PJ domain, leading to reactions such as mitophagy. The results herein indicate that the N-terminus is the principle functional domain of MAP4, therefore this may also be the case for other MAP family members.

This study also demonstrates that MAP4 is a cargo receptor of mitophagy in cardiomyocytes through its characteristic LIR domain and specifically interacts with LC3. Under both physiological and hypoxic conditions, MAP4 impacts mitophagy after its phosphorylation at S737 and S760, resulting in increased co-localisation and interaction of MAP4/LC3. This leads to the selective mitochondrial incorporation into LC3-bound isolation membranes for the subsequent removal of mitochondria. It is noteworthy that mitophagic cargo receptors use LIR or UIM motif that associates with the LDS or UDS site on LC3, respectively, which culminates in the formation of mitophagosomes[6, 8, 28]. Importantly, canonical LIR and UIM motifs were found within the MAP4 PJ domain (Fig. 3C and 3H). However, detailed interaction experiments confirmes that only the MAP4 LIR motif (47–50aa) is responsible for LC3/MAP4 interactions, mitochondrial engulfment and mitochondrial degradation (Fig. 3). This underlies the structural foundation for p-MAP4-induced mitophagy. Our findings thus provide insights into how MAP4 acts as a mitophagy receptor to couple with the core autophagic machinery and how MAP4-dependent mitophagy is regulated by phosphorylation.

In this article, MAP4-induced mitophagy was shown to be structure and potential-independent. Phagophore formation and mitochondrial recognition are therefore the key aspects of these mechanisms,

of which MAP4 was shown to stimulate the former, resulting in phagophore over-accumulation. In turn, the over-accumulation of phagophores make the cells unable to accurately distinguish healthy from impaired mitochondria. In fact, a UIM domain is found in MAP4, which is notable since UIM domain leads to the ubiquitination of mitochondrial membrane proteins and functions as the bridge between them and proteins in phagophores[6, 8]. Therefore, proteins with canonical UIM domains, other than MAP4, may also induce mitophagy in a structure- and potential-independent manner.

Based upon its distribution and structural status, and the results from this study, combined with the fact that MAP4 is conserved in higher eukaryotic organisms and ubiquitously expressed in non-neural cells[12–13], MAP4 appears to be a qualified cargo receptor in mitophagy. However, some differences exist between MAP4 and other known mitophagy cargo receptors. Traditionally, NIX and FUNDC1 are involved in hypoxia-induced autophagy and are indispensable for the programmed elimination of mitochondria during reticulocyte maturation [29]. Yet, based upon our findings the mechanism of MAP4-induced mitophagy is distinct from that of NIX or FUNDC1. Unlike NIX or FUNDC1, MAP4 contains BH3, LIR, and UIM domains, indicating it can function in the entire process of autophagy (including autophagy activation and cargo recognition) by itself. Additionally, whilst all these proteins are involved in hypoxia induced mitophagy, the expression of NIX or FUNDC1 is altered, whereas MAP4 remains unchanged. However, unlike FUNDC1, both Nix and MAP4 are distributed in other organelles under physiological conditions and are involved in regulation of mitochondrial apoptosis under hypoxia conditions[18,30]. Therefore, whilst the roles of MAP4, NIX, and FUNDC1 in the induction of mitophagy are different to some extent, they probably cooperate with each other during this process.

Based upon the results contained herein, the increased and decreased MAP4 phosphorylation, accelerates or mitigates (respectively) hypoxia-induced mitophagy impairment (Fig. 6). This is precedented given that the activity of MAPT/Tau (MAP4 a family member) is also known to disrupt autophagic flux[31]. Abnormal mitophagy has been closely associated with heart failure, ischemia-reperfusion injury and cardiac hypertrophy[30]. Considering that the mechanism of MAP4-related cardiac hypertrophy and ischemic heart failure remains obscure, this study provides powerful evidence to support this notion. This article defines MAP4 as a potential mediator in cardiac dysfunction, including hypertrophy and heart failure.

We et al [17] and Yu et al [19] demonstrated that MAP4 influences cardiac pathology, including cardiac hypertrophy and ischemic heart failure. Therefore, it is possible that the MAP4 PJ domain might be the primary region responsible for these effects. Moreover, the results reported herein could explain the mechanism of MAP4-induced myocardial damage and ischemic heart failure, which has profound biological and clinical implications. Additionally, the current study indicates that the MAP4 PJ domain is the core functional region of MAP4 in mitophagy, and it can be successfully synthesised and used *in vitro*. However, further research is required to determine the precise influence of the MAP4 PJ domain on heart failure or cardiac remodelling and to fully clarify the relevance of the MAP4 PJ domain in other diseases. Nevertheless, the MAP4 PJ domain appears to be a promising therapeutic target for a

degradation strategy, which could have considerable potential for the treatment/prevention of hypoxia-related myocardial damage and heart failure.

Materials And Methods

Ethics statement

All animal experiments were carried out according to the guidelines of the Care and Use of Laboratory Animal (NIH Pub. 8th edition, 2011) and authorized by the Animal Experiment Ethics Committee of the Army Medical University (the Third Military Medical University) in Chongqing, China.

Animal studies

The *MAP4* (S667A, S737E, and S760E)-KI mice were generated and bred as previously described [17]; wild-type (C57BL6/J) mice were purchased from the Animal Centre, Army Medical University (Third Military Medical University, CHN). Male mice, 8-10-weeks-old and weighing 18-22 g, were used for the experiments. The mice were fed a standard rodent chow diet, allowed access to water *ad libitum*, and housed under 12-hour light/dark cycles. Prior to the experiments, all animals were allowed to acclimate to the facility for one week. The animals were randomly divided into four groups, control, *MAP4*-KI, hypoxia, and hypoxia+*MAP4* KI. Hypoxia was induced with 7.5% O_2, 0.1% CO_2 and 92.5% N_2 for seven days. The desired temperature (22℃) was maintained using a Forma Series II Water Jacket CO_2 incubator (model 3131; Thermo Fischer Scientific, Waltham, MA, USA) and the O_2 level was controlled through a continuous flow of nitrogen. Afterward, the mice were immediately euthanised, and their heart tissues were collected for transmission electron microscopy or western blot analysis.

Primary cardiomyocytes culture and Hypoxia

Primary cardiomyocytes were isolated according to the conventional methods of our group [11]. Firstly, neonatal C57BL6/J or *MAP4* KI mice (1-2 days old) were obtained. The hearts were digested with trypsin and collagenase, and then cultured in 6, 24 and 96-well culture plates and maintained for 72 h in Dulbecco's Modified Eagle's Medium (DMEM)-F12 (HyClone) containing 5-bromodeoxyuridine (BrdU; 31mg/L), 10% fetal bovine serum (FBS; Gibco) and penicillin (100U/mL). The primary cardiomyocytes were incubated at 37℃, 5% CO2, and 95% humidity. Hypoxia was induced with 1% O2, 5% CO2, and 94% N2. The desired temperature (37℃) and O_2 level were maintained by a Forma Series II Water Jacket CO2 incubator (model: 3131; Thermo Scientific) through a continuous flow of nitrogen.

Mitochondria fractions preparation

Mitochondrial fractions were prepared and validated from primary cardiomyocytes according to the manual instruction of Cell Fractionation Kit (Abcam, ab109719). Briefly, primary cardiomyocytes were collected, counted and diluted to 6.6*10^6 cell/mL. Then, after centrifuged at 500g at 4℃ for 1min, the supernatant was collected and again centrifuged at 10000g at 4℃ for 1min. Then, the pellets were

collected and resuspend, and after same centrifugation process, the supernatants containing mitochondrial proteins were collected.

Western blot (WB) analysis

The proteins were extracted as previously reported [11]. Briefly, samples were harvested using lysis buffer containing a protease inhibitor, phosphatase inhibitor and PMSF (Beyotime, China). After quantitated with Quick Start™ Bradford 1×Dye Reagent (Bio-Rad, USA), the protein extracts were separated using sodium dodecyl sulfate-polyacrylamide gel electrophoresis (SDS-PAGE) (Bio-Rad, USA), and then transferred to polyvinylidene fluoride (PVDF) membranes (Bio-Rad, USA). Furthermore, the dissected PVDF membranes were incubated overnight at 4℃ with the following primary antibodies: LC3 (Sigma, 1:2000), Atg3 (CST, 1:1000), Atg7 (CST, 1:1000), Beclin1 (CST, 1:1000), Atg16L1 (CST, 1:1000), Atg5-Atg12 (CST, 1:1000), Bcl-2 (abcam, 1:1000), p62 (Invitrogen, 1:1000), SERCA2 (abcam, 1:1000), Golgin97 (proteintech, 1:1000), HSP60(abcam, 1:1000), Tom70 (Santa Cruz, 1:500), HA tag (proteintech, 1:1000), p-MAP4 (1:1000), MAP4 (Affinity, 1:1000), p-MAP4 (S768) (Biolegend, 1:5000), p-MAP4 (S787) (GL Biochem, 1:1000), p-MAP4 (S737) (GL Biochem, 1:1000), ubiquitin (CST, 1:1000) and β-actin (Proteintech, 1:5000). After successively incubating with horseradish peroxidase-conjugated secondary antibodies and an enhanced chemiluminescence detection kit (Amersham Pharmacia, Piscataway, NJ), the PVDF membranes were visualized and quantified using ChemiDoc XRS system (Bio-Rad, Hercules, CA, United States) and Quantity One software (Bio-Rad), respectively.

Transmission Electron Microscope (TEM)

The procedure of this part was according to previous experiment [17]. After fixed in 2.5% glutaraldehyde, primary cardiomyocytes or left ventricle (LV) myocardium were successively subjected to dehydration, vibratome sliced and recut on a microtome and stained with uranyl acetate and lead citrate overnight. The sections were visualized through a TEM (JEM-1400 plus, Japan).

Co-immunoprecipitation

To address the interaction between MAP4/Bcl-2, MAP4/LC3, Bcl-2/Beclin1, and MAP4/Ubiquitin. Cardiomyocytes were lysed in RIPA buffer with a protease inhibitor tablets. The MAP4, Bcl-2, Ubiquitin or LC3 antibodies were incubated with cell lysate for 24 h at 4 °C, then the samples were precipitated with protein A/G-Sepharose (Santa Cruz, Cat# sc-2003) overnight at 4 °C. The precipitates were washed 5 times with PBS at 0 °C and separated by SDS-PAGE and probed by rabbit anti-MAP4 (1:1000, Affinity, USA), anti-LC3 (Sigma, 1:2000), anti-Beclin1 (CST, 1:1000), anti-Bcl-2 (CST, 1:2000) and anti-ubiquitin (CST, 1:1000) antibodies using WB.

Immunofluorescence Staining

The immunofluorescence was performed as previously reported[17]. Cardiomyocytes were fixed with 1% paraformaldehyde and then permeabilized in 1% Triton X-100 (Sigma, T9284). The nonspecific binding

sites were blocked with 10% normal goat serum for 60 min. Cells were stained with p-MAP4 antibody at 1:100, and fluorescence conjugated secondary antibodies: Alexa Fluor 488-conjugated goat anti-rabbit IgG antibody (Invitrogen) at 1:100 and Alexa Fluor 561-conjugated goat anti-mouse IgG antibody at 1:100. To detect mitochondrial membrane potential, the living cells are stained with TMRE (200nmol/L) for 20min. The cells were viewed and analyzed through a TCS SP5 laser confocal microscope (CANT; Leica, Wetzlar, Germany) or Leica LAS AF 2.3.0 software (Leica Microsystems, Germany), respectively.

RFP-LC3, GFP-LC3, mRFP-GFP-LC3 and Dsred-Mito adenoviruses

The mRFP-GFP-LC3, mRFP-LC3, GFP-LC3 and Dsred-Mito adenovirus were purchased from Hanbio Biotechnology (Shanghai, China) to respectively detect autophagy flux and mitophagosome. The cardiomyocytes grown on glass coverslips in 24-well plates were transferred with these adenoviruses overnight before corresponding treatment, and then the slides were visualized using a confocal microscope (CANT; Leica, Wetzlar, Germany).

HSP60, Tom70 and MARK4 gene silencing with siRNAs

HSP60, Tom70 and MARK4 siRNAs were purchased from GenePharma (Shanghai, China). Cardiomyocytes were transferred with negative control siRNA or HSP60 or Tom70 or MARK4 siRNAs using Lipofectamine 2000 (Nitrogen, USA) according to the manufacturer's protocol. The cells were maintained for 24 h and then used in subsequent experiments.

Bcl-2, MAP4 (Ala), MAP4 (Glu), MAP4 (PJ), UIM-mutated MAP4 (Glu), LIR-mutated MAP4 (Glu) and BH3-mutated MAP4 (Glu) recombinant adenovirus construction and transduction

Recombinant adenovirus vectors were used to overexpress Bcl-2, MAP4 PJ domain (1–693 aa, S737/S760E), UIM-mutated MAP4 (Glu) (L468/S475A and S737/ S760E), LIR-mutated MAP4 (Glu) (Y34/I37A and S737/ S760E), LIR-mutated MAP4 (Glu) (F47/L50A and S737/ S760E), and BH3-mutated MAP4 (Glu) (L83/G87/D88A and S737/S760E). These adenoviruses were constructed by and purchased from the GeneChem Company (CHN). Furthermore, the adenoviruses encoding the MAP4 (Glu) (S737E and S760E) and MAP4 (Ala) (S737A and S760A) were produced as previously described[16,17]. Cardiomyocytes, cultured in 6, 24 or 96 well plates, were transduced with the corresponding adenoviruses for 48 hours, the transfection efficiency was assessed by WB.

GST pull-down assay

GST pull-down assays were performed by GeneCreate Biological Engineering CO., Ltd (CHN). In brief, the *LC3*, *MAP4 PJ1* (*1-170aa*), *MAP4 PJ2* (*398-547aa*), *MAP4 PJ1 LIR$^{\triangle 34,37}$* or *MAP4 PJ2 LIR$^{\triangle 47,50}$* genes were first inserted into PGEX-6P-1 and pet-sumo vectors. The five recombinant plasmids were subsequently expressed in *Escherichia coli*, followed by the purification of GST-*LC3*, HIS-*MAP4 PJ1*, HIS-*MAP4 PJ2*, HIS- *MAP4 PJ1 LIR$^{\triangle 34,37}$*, and HIS- *MAP4 PJ2 LIR$^{\triangle 47,50}$*. The GST pull-down was conducted according to a previous published protocol [32] and measured via western blotting.

Qualitative (shotgun) protein analysis

Cardiomyocytes were lysed in RIPA buffer containing protease inhibitors. The MAP4 antibody was incubated with the cell lysates for 24 hours at 4 °C, and the samples were precipitated with protein A/G-Sepharose (Cat# sc-2003, RRID: AB_10201400; Santa Cruz Biotechnology, USA) overnight at 4 °C. The precipitates, after five washing steps with PBS at 0 °C, were analysed via label-free shotgun proteomics. In brief, sample preparation, protein digestion, in-gel digestion, liquid chromatography-electrospray ionisation tandem MS analysis (Q Exactive) and sequence database searching and data analysis were performed. The MS data was searched against the Uniport database. Intensity-based absolute quantification (iBAQ) with MaxQuant was performed on the identified peptides to quantify the protein abundance.

Statistical analysis

All data are presented was presented using the mean ± SEM. The statistical analysis was performed using SPSS, v. 22.0. The independent-sample *t*-test and the one-way analysis of variance were applied for comparisons between two groups or more than two groups, respectively. Pearson's correlation coefficient was calculated using Image J (Fiji) software. P=<0.05 (two tailed) was used as the threshold to define statistical significance.

Declarations

Acknowledgements and Funding

This study was supported by the Key Project of National Natural Science Foundation of China (NSFC) (No. 81430042), the State Key Laboratory of Trauma, Burns and Combined Injury Research Foundation (No. SKLYQ201802), and the National Youth Fund Project of China (No. 82003323).

Author contributions

Conceptualization, Yanhai Feng, Jiongyu Hu, Yuesheng Huang and Gaoxing Luo; Methodology, Yanling Lv, Jiezhi Jia and Dongxia Zhang; Software, Yanling Lv, Jiezhi Jia, Dongxia Zhang and Yao Huang; Validation, Junhui Zhang, Yanhai Feng; Formal Analysis, Yanhai Feng, Junhui Zhang, Lingfei Li; Investigation, Jiongyu Hu.; Resources, Yanhai Feng; Data Curation, Yanhai Feng, Qiong Zhang; Writing – Original Draft Preparation, Yanhai Feng and Qiong Zhang; Writing – Review & Editing, Jiongyu Hu, Gaoxing Luo and Yuesheng Huang; Visualization, Jiongyu Hu and Yuesheng Huang; Supervision, Jiongyu Hu and Yuesheng Huang; Project Administration, Jiongyu Hu and Yuesheng Huang; Funding Acquisition, Jiongyu Hu and Yuesheng Huang.

Conflict of Interest

The authors declare that they have no conflicts of interest.

References

1. Thomas RL, Kubli DA, Gustafsson ÅB. Bnip3-mediated defects in oxidative phosphorylation promote mitophagy. *Autophagy* 2011;**7**:775–777.
2. Geisler S, Holmström KM, Skujat D, Fiesel FC, Rothfuss OC, Kahle PJ, Springer W. PINK1/Parkin-mediated mitophagy is dependent on VDAC1 and p62/SQSTM1. *Nat Cell Biol* 2010;**12**:119–131.
3. Novak I, Kirkin V, McEwan DG, Zhang J, Wild P, Rozenknop A, Rogov V, Löhr F, Popovic D, Occhipinti A, Reichert AS, Terzic J, Dötsch V, Ney PA, Dikic I. Nix is a selective autophagy receptor for mitochondrial clearance. *EMBO Rep*. 2010;**11**:45–51.
4. Hanna RA, Quinsay MN, Orogo AM, Giang K, Rikka S, Gustafsson ÅB. Microtubule-associated protein 1 light chain 3 (LC3) interacts with BNIP3 protein to selectively remove endoplasmic reticulum and mitochondria via autophagy. *J Biol Chem* 2012;**287**:19094–19104.
5. Liu L, Feng D, Chen G, Chen M, Zheng Q, Song P, Ma Q, Zhu C, Wang R, Qi W, Huang L, Xue P, Li B, Wang X, Jin H, Wang J, Yang F, Liu P, Zhu Y, Sui S, Chen Q. Mitochondrial outer-membrane protein FUNDC1 mediates hypoxia-induced mitophagy in mammalian cells. *Nat Cell Biol* 2012;**14**:177–185.
6. C.T. Chu, J. Ji, R.K. Dagda, J.F. Jiang, Y.Y. Tyurina, A.A. Kapralov, V.A. Tyurin, N. Yanamala, I.H. Shrivastava, D. Mohammadyani, K.Z. Qiang Wang, J. Zhu, J. Klein-Seetharaman, K. Balasubramanian, A.A. Amoscato, G. Borisenko, Z. Huang, A.M. Gusdon, A. Cheikhi, E.K. Steer, R. Wang, C. Baty, S. Watkins, I. Bahar, H. Bayır, V.E. Kagan, Cardiolipin externalization to the outer mitochondrial membrane acts as an elimination signal for mitophagy in neuronal cells, *NAT. CELL BIOL.* **15**, 1197–1205(2013).
7. R.S. Marshall, Z. Hua, S. Mali, F. McLoughlin, R.D. Vierstra, ATG8-binding UIM proteins define a new class of autophagy adaptors and receptors, *CELL*, **177**, 766–781(2019).
8. D. Fracchiolla, J. Sawa-Makarska, B. Zens, A.D. Ruiter, G. Zaffagnini, A. Brezovich, J. Romanov, K. Runggatscher, C. Kraft, B. Zagrovic, S. Martens, Mechanism of cargo-directed Atg8 conjugation during selective autophagy, *ELIFE*, **5**(2016).
9. Huang J, Li R, Wang C. The Role of mitochondrial quality control in cardiac Ischemia/Reperfusion injury. *Oxid Med Cell Longev*,2021(2021)10 N. Mohan, E.M. Sorokina, I.V. Verdeny, A.S. Alvarez, M. Lakadamyali, Detyrosinated microtubules spatially constrain lysosomes facilitating lysosome-autophagosome fusion, *J. CELL BIOL.***218**, 632-643(2019).
10. L. Yang, L. Zhao, L. Cui, Y. Huang, J. Ye, Q. Zhang, X. Jiang, D. Zhang, Y. Huang, Decreased α-tubulin acetylation induced by an acidic environment impairs autophagosome formation and leads to rat cardiomyocyte injury, *J. MOL. CELL. CARDIOL.* **127**, 143–153(2019).
11. J. Hu, Z. Chu, J. Han, Y. Dang, H. Yan, Q. Zhang, G. Liang, Y. Huang, The p38/MAPK pathway regulates microtubule polymerization through phosphorylation of MAP4 and Op18 in hypoxic cells, *CELL. MOL. LIFE SCI.* **67**, 321–333(2010).
12. L. Li, J. Hu, T. He, Q. Zhang, X. Yang, X. Lan, D. Zhang, H. Mei, B. Chen, Y. Huang, P38/MAPK contributes to endothelial barrier dysfunction via MAP4 phosphorylation-dependent microtubule

disassembly in inflammation-induced acute lung injury, *SCI REP-UK*, **5**(2015).

13. G. Drewes, A. Ebneth, E. Mandelkow, MAPs, MARKs and microtubule dynamics, *TRENDS BIOCHEM. SCI.* **23**, 307–311(1998).
14. Iida J, Itoh TJ, Hotani H, Nishiyama K, Murofushi H, Bulinski JC, Hisanaga S. The projection domain of MAP4 suppresses the microtubule-bundling activity of the microtubule-binding domain. *J Mol Biol* 2002;**320**:97–106.
15. Katsuki M, Tokuraku K, Murofushi H, Kotani S. Functional analysis of microtubule-binding domain of bovine MAP4. *Cell Struct Funct* 1999;**24**:337–344.
16. Li L, Zhang Q, Zhang X, Zhang J, Wang X, Ren J, Jia J, Zhang D, Jiang X, Zhang J, Mei H, Chen B, Hu J, Huang Y. Microtubule associated protein 4 phosphorylation leads to pathological cardiac remodeling in mice. *Ebiomedicine* 2018;**37**:221–235.
17. Hu J, Chu Z, Han J, Zhang Q, Zhang D, Dang Y, Ren J, Chan HC, Zhang J, Huang Y. Phosphorylation-dependent mitochondrial translocation of MAP4 is an early step in hypoxia-induced apoptosis in cardiomyocytes. *Cell Death Dis* 2014;**5**:e1424.
18. X. Yu, X. Chen, M. Amrute-Nayak, E. Allgeyer, A. Zhao, H. Chenoweth, M. Clement, J, Harrison, C. Doreth, G. Sirinakis, T. Krieg, H. Zhou, H. Huang, K, Tokuraku, D. st Johnston, Z. Mallat, X. Li. MARK4 controls ischemic heart failure through microtubule detyrosination. *Nature*, **594**, 560–565 (2021).
19. Peng F, Zhang N, Wang C, Wang X, Huang W, Peng C, He G, Han B. Aconitine induces cardiomyocyte damage by mitigating BNIP3-dependent mitophagy and the TNFα-NLRP3 signaling axis. *Cell Proliferat* 2019;**53**.
20. Maiuri MC, Le Toumelin G, Criollo A, Rain J, Gautier F, Juin P, Tasdmir E, Pieeron G, Troulinaki K, Tavarnarakis N, Hichman JA, Geneste O, Kroemer G. Functional and physical interaction between Bcl-XL and a BH3-like domain in Beclin-1. *EMBO J* 2007;**26**:2527–2539.
21. Fracchiolla D, Sawa-Makarska J, Zens B, Ruiter AD, Zaffagnini G, Brezovich A, Romanov J. Mechanism of cargo-directed Atg8 conjugation during selective autophagy. *eLife* 2016;**23**:5.
22. Morciano G, Patergnani S, Bonora M, Pedriali G, Tarocco A, Bouhamida E, March S, Ancora G, Anania G, Wieckowski MR, Giorgi C, Pinton P. Mitophagy in cardiovascular diseases. *J Clin Med* 2020;**9**:892.
23. Ren J, Sun M, Zhou H, Ajoolabady A, Zhou Y, Tao J, Sowers JR, Zhang Y. FUNDC1 interacts with FBXL2 to govern mitochondrial integrity and cardiac function through an IP3R3-dependent manner in obesity. *Sci Adv* 2020; 6:38.
24. Yu Y, Sun B. Autophagy-mediated regulation of neutrophils and clinical applications. Burns Trauma 2020;8:tkz001.
25. Kronlage M, Dewenter M, Grosso J, Fleming T, Oehl U, Lehmann LH, Falcão-Pires I, Leite-Moreira AF, Volk N, Gröne HJ, Müller OJ, Sickmann A, Katus HA, Backs J. O-GlcNAcylation of histone deacetylase 4 protects the diabetic heart from failure. *Circulation* 2019;**140**:580–594.
26. L. Liu, K. Sakakibara, Q. Chen, K. Okamoto, Receptor-mediated mitophagy in yeast and mammalian systems, *CELL RES.*, **24**, 787–795(2014).

27. T. Johansen, T. Lamark, Selective autophagy mediated by autophagic adapter proteins, *AUTOPHAGY*, **7**, 279–296(2011).
28. L. Liu, D. Feng, G. Chen, M. Chen, Q. Zheng, P. Song, Q. Ma, C. Zhu, R. Wang, W. Qi, L. Huang, P. Xue, B. Li, X. Wang, H. Jin, J. Wang, F. Yang, P. Liu, Y. Zhu, S. Sui, Q. Chen, Mitochondrial outer-membrane protein FUNDC1 mediates hypoxia-induced mitophagy in mammalian cells, *NAT. CELL BIOL.*, **14**, 2 (2012).
29. Doblado L, Lueck C, Rey C, Samhan-Arias AK, Prieto I, Stacchiotti A and Monsalve M. Mitophagy in human diseases. *Int J Mil Sci*, **22**,8 (2021).
30. Q. Feng, Y. Luo, X.N. Zhang, X.F. Yang, X.Y. Hong, D.S. Sun, X.C. Li, Y. Hu, X.G. Li, J.F. Zhang, X. Li, Y. Yang, Q. Wang, G.P. Liu, J.Z. Wang, MAPT/Tau accumulation represses autophagy flux by disrupting IST1-regulated ESCRT-III complex formation: a vicious cycle in Alzheimer neurodegeneration, *AUTOPHAGY*, **16**, 641–658(2020).
31. Huang Y, Feng Y, Cui L, Yang L, Zhang Q, Zhang J, Jiang X, Zhang X, Lv Y, Jia JZ, Zhang DX, Huang YS. Autophagy-Related LC3 Accumulation Interacted Directly With LIR Containing RIPK1 and RIPK3, Stimulating Necroptosis in Hypoxic Cardiomyocytes. *Front Cell Dev Biol*, 9 (2021).

Figures

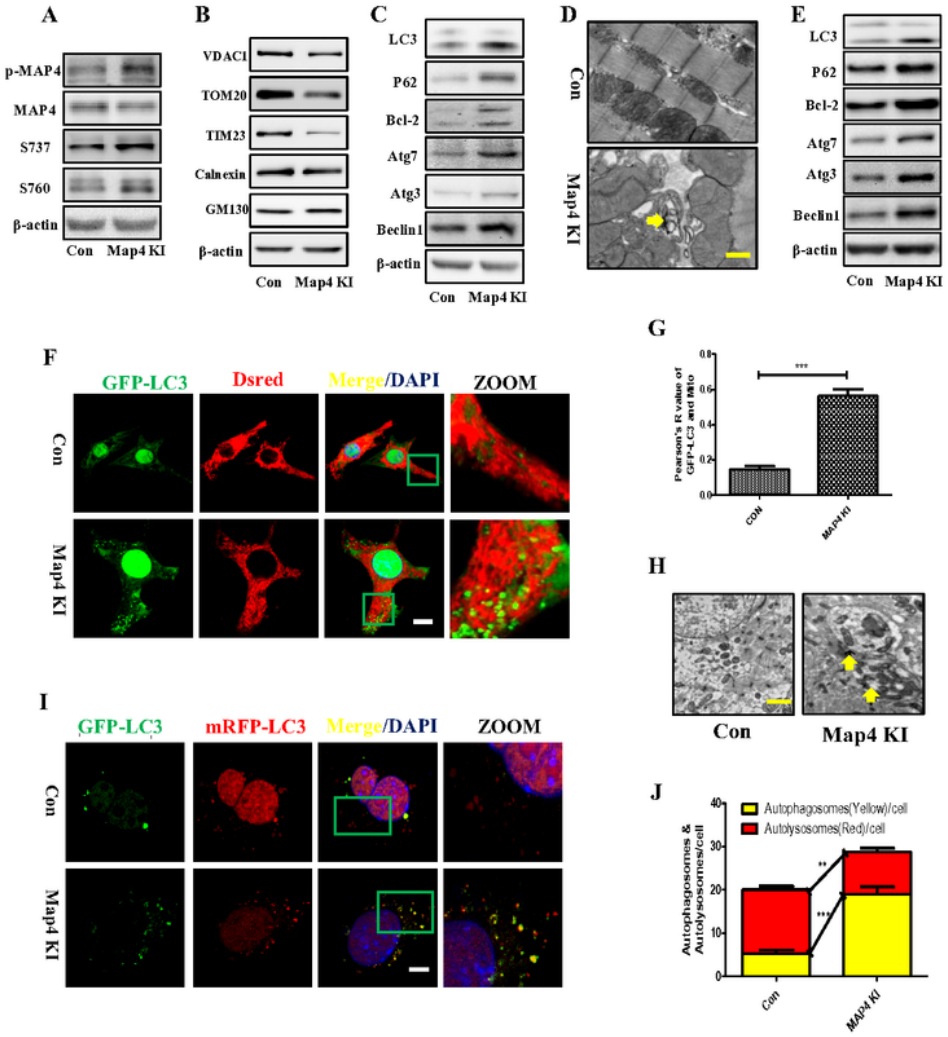

Figure 1

Increased p-MAP4 degrades mitochondria through impacting mitophagy in the whole life of mice. (A). The myocardium specimens of MAP4- KI mice were used to verify whether it is an effective p-MAP4 model. MAP4, p-MAP4, p-MAP4 (S737), and p-MAP4 (S760) were detected. n=5. (B) The myocardium specimens of MAP4 KI mice were used to detect VDAC1, Tom20, TIM23, Calnexin, GM130. (C). The MAP4-KI myocardium was used to measure LC3, p62, BCL-2, Atg7, Atg3, and Beclin1. n=5. (D).

Representative images of mitophagosomes in the MAP4-KI myocardium. Yellow arrows point to mitophagosomes. Scale bar=1 μm. n=3. (E). The primary cardiomyocytes of MAP4-KI mice were used to detect autophagy-related proteins, including LC3, p62, Bcl-2, Atg7, Atg3, Atg16L1, and Beclin1. n=5. (F). Representative images of mitophagosome, detected by co-staining with GFP-LC3 and Dsred-Mito, in the primary cardiomyocytes of MAP4-KI mice. Scale bar=10 μm. n=3. (G). Statistical analysis of Pearson's R value in (E). ***$p<0.001$ versus the Con group. n = 3. (H). Representative images of mitophagosome, detected by TEM, in primary cardiomyocytes of MAP4-KI mice. Yellow arrows point to mitophagosome. Scale bar= 0.5 μm. n = 3. (I). Representative images of autophagy flux, detected by mRFP-GFP-LC3, in the primary cardiomyocytes of MAP4-KI mice. Scale bar=10 μm. n = 3. (J) Statistical analysis of autophagosomes and autolysosomes in (H). **$p<0.01$ and ***$p<0.001$ versus the Con group. n=3.

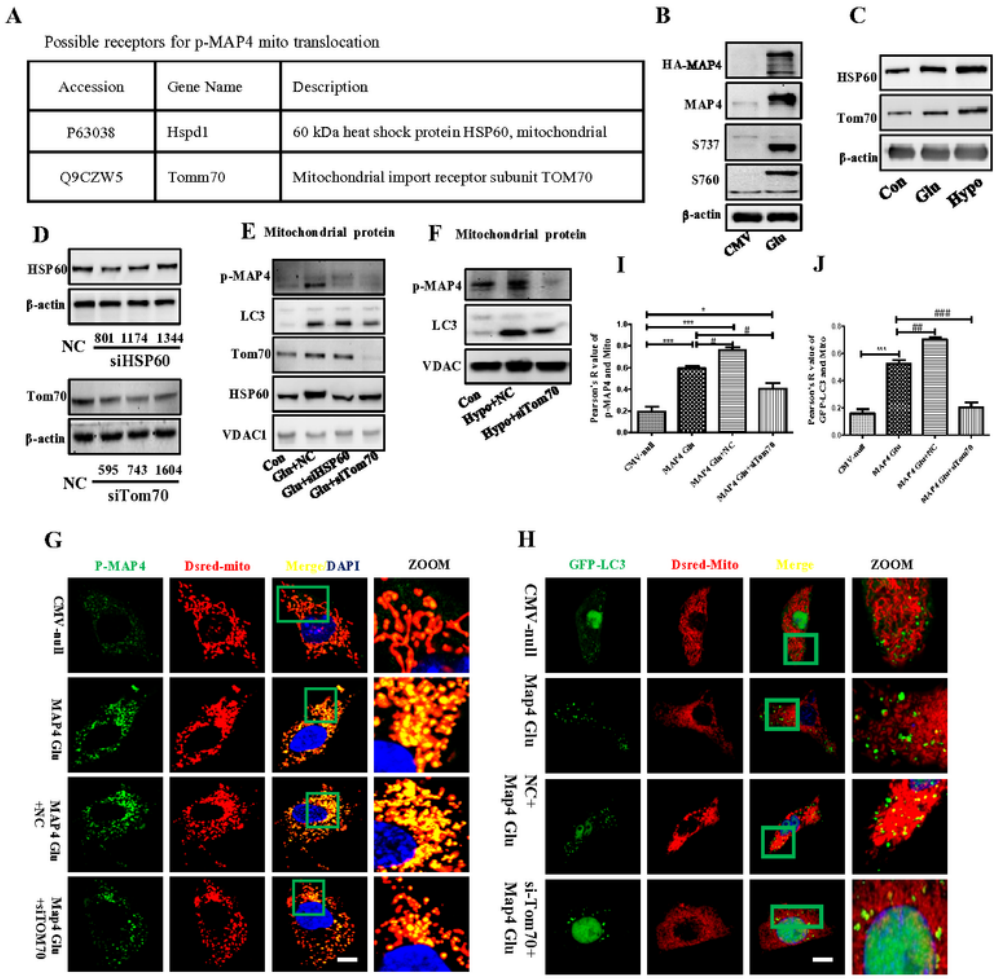

Figure 2

Tom70 mediates the mitochondrial translocation of p-MAP4. (A) Possible importers of MAP4 mitochondrial translocation analysed by protein qualitative (shotgun) analysis. (B) Detection of transfection efficiency of Ad-MAP4 (Glu) in primary cardiomyocytes. n=5. (C) Representative bands of HSP60 and Tom70 in cardiomyocytes. n=5. (D) Transfection efficiency of HSP60 and Tom70 siRNAs. (E) Representative bands for p-MAP4, LC3, Tom70, and HSP60 in mitochondrial proteins after treatment with

Ad-MAP4 (Glu) with or without Tom70 siRNA. n=5. (F) Representative bands of p-MAP4 and LC3 in mitochondrial proteins after treatment with hypoxia with or without Tom70 siRNA. n=5. (G) Representative images of co-localisation of p-MAP4 and mitochondria in cardiomyocytes. Scale bar=10 μm. n=3. (H) Representative images of mitophagosomes in cardiomyocytes treated with Ad-MAP4 (Glu) with or without Tom70 siRNA. Scale bar=10 μm. n=3. (I) Statistical analysis of Person's value in (F). *p<0.05 and ***p<0.001 versus CMV-null group; #p<0.05 versus MAP4 (Glu) group. n=3. (J) Statistical analysis of Pearson's R value of GFP-LC3 and dsred-mito in (G). ***p<0.001 versus CMV-null group; ##p<0.01 and ###p<0.001 versus MAP4 Glu group. n=3.

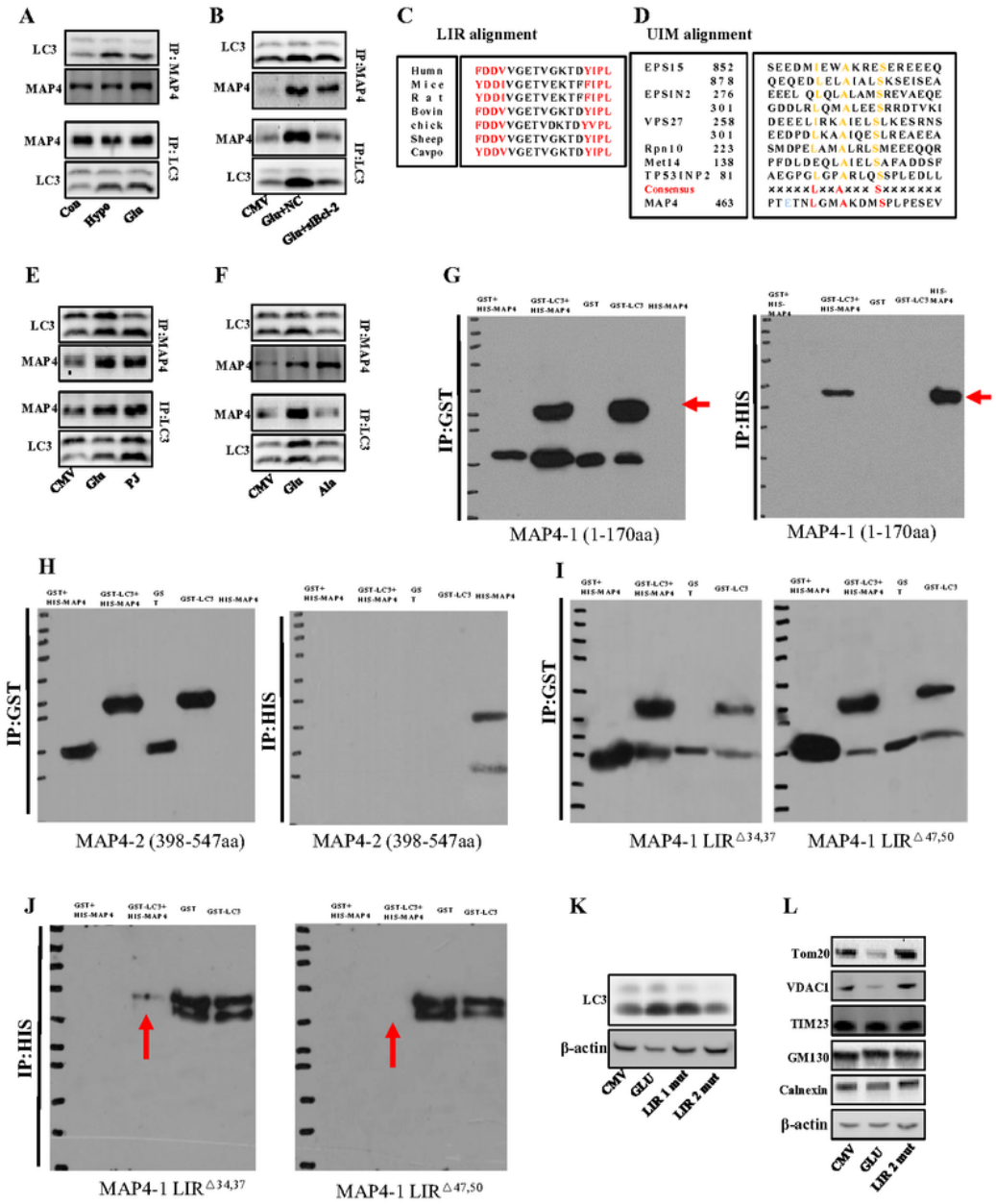

Figure 3

The LIR (47–50aa) in MAP4 determines mitochondrial engulfment and degradation (A-B) Cardiomyocyte specimens were lysed and immunoprecipitated with anti-LC3 or anti-MAP4 antibodies followed by WB with anti-LC3 and anti-MAP4 antibodies. n=3. (C) LIR alignment of MAP4. (D) UIM alignment of MAP4. (E-F) Cardiomyocyte specimens were lysed and immunoprecipitated with anti-LC3 or anti-MAP4 antibodies followed by western blotting with anti-LC3 and anti-MAP4 antibodies. n=3. (G) The direct interaction of

GST-LC3 and HIS-MAP4-1 measured by GST-pull down. n=3. (H) The direct interaction of GST-LC3 and HIS-MAP4-2 detected by GST-pull down. n=3. (I, J) The direct interaction of LC3 antibody and MAP4-1 LIR△34,37 or MAP4-1 LIR△47,50 detected by GST or HIS antibody. n=3. (K) The representative band of LC3 in primary cardiomyocytes incubated with Ad-MAP4 (Glu), Ad-LIR1 mutated MAP4 (Glu) and Ad-LIR2 mutated MAP4 (Glu). n=3. (L) The representative bands of Tom20, VDAC1, TIM23, GM130 and Calnexin in the primary cardiomyocytes incubated with Ad-MAP4 (Glu) and Ad-LIR2 mutated MAP4 (Glu). n=3.

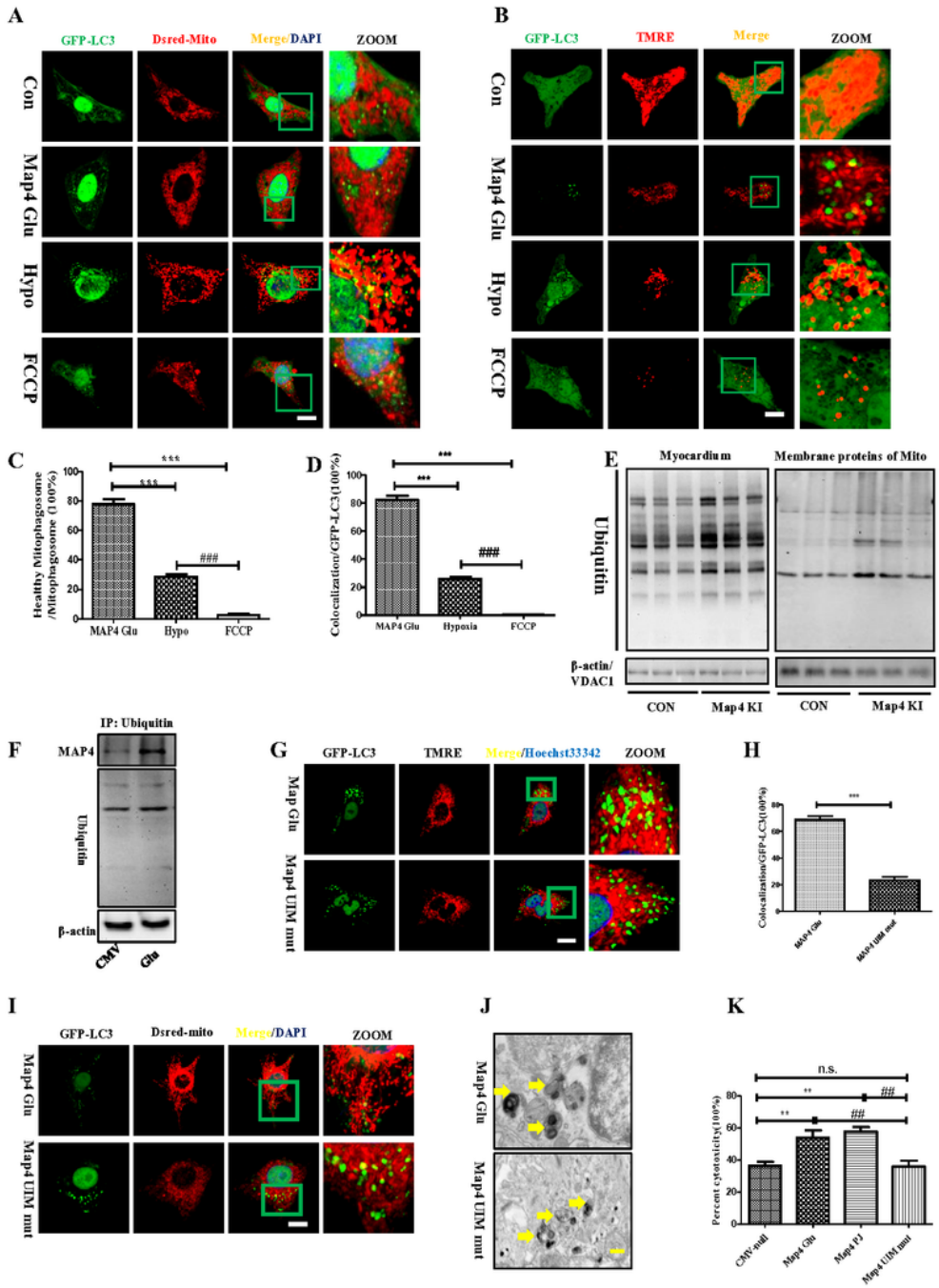

Figure 4

The UIM domain maintains the specific characteristics of p-MAP4 induced mitophagy. (A) Representative images of co-localisation of GFP-LC3 and Dsred-Mito in cardiomyocytes treated with Ad-MAP4 (Glu), hypoxia, or FCCP. Scale bar=10 μm. n=3. (B) Representative images of GFP-LC3 and TMRE in cardiomyocytes treated with Ad-MAP4 (Glu), hypoxia, or FCCP. Scale bar=10 μm. n=3. (C) Proportion of mitophagosomes induced by p-MAP4 among mitophagosomes based on (A). ***p<0.001 versus Ad-MAP4 (Glu) group; ###p<0.001 versus hypoxia group. n=5. (D) Proportion of GFP-LC3/TMRE co-localisation in GFP-LC3 based on (B). ***p<0.001 versus Ad-MAP4 (Glu) group; ###p<0.001 versus hypoxia group. n=5. (E) Representative membranes of ubiquitin in myocardium or mitochondrial proteins of MAP4-KI mice. n=3. (F) Cardiomyocyte specimens were lysed and immunoprecipitated with an anti-ubiquitin antibody followed by WB with anti-MAP4. n=3. (G) Representative images of GFP-LC3 and TMRE in cardiomyocytes. Scale bar=10 μm. n=3. (H) Statistical analysis of co-localisation in (G). ***p<0.001 versus con group. n=5. (I) Representative images of mitophagosomes in cardiomyocytes. Scale bar=10 μm. n=3. (J) Representative images of mitophagosomes measured by TEM in cardiomyocytes. Scale bar=1 μm. n=3. (K) Histogram of cellular cytotoxicity in cardiomyocytes. **p<0.01 versus CMV-null group. ##p<0.01 versus MAP4 (Glu) group. n.s. means without a statistical difference. n=5.

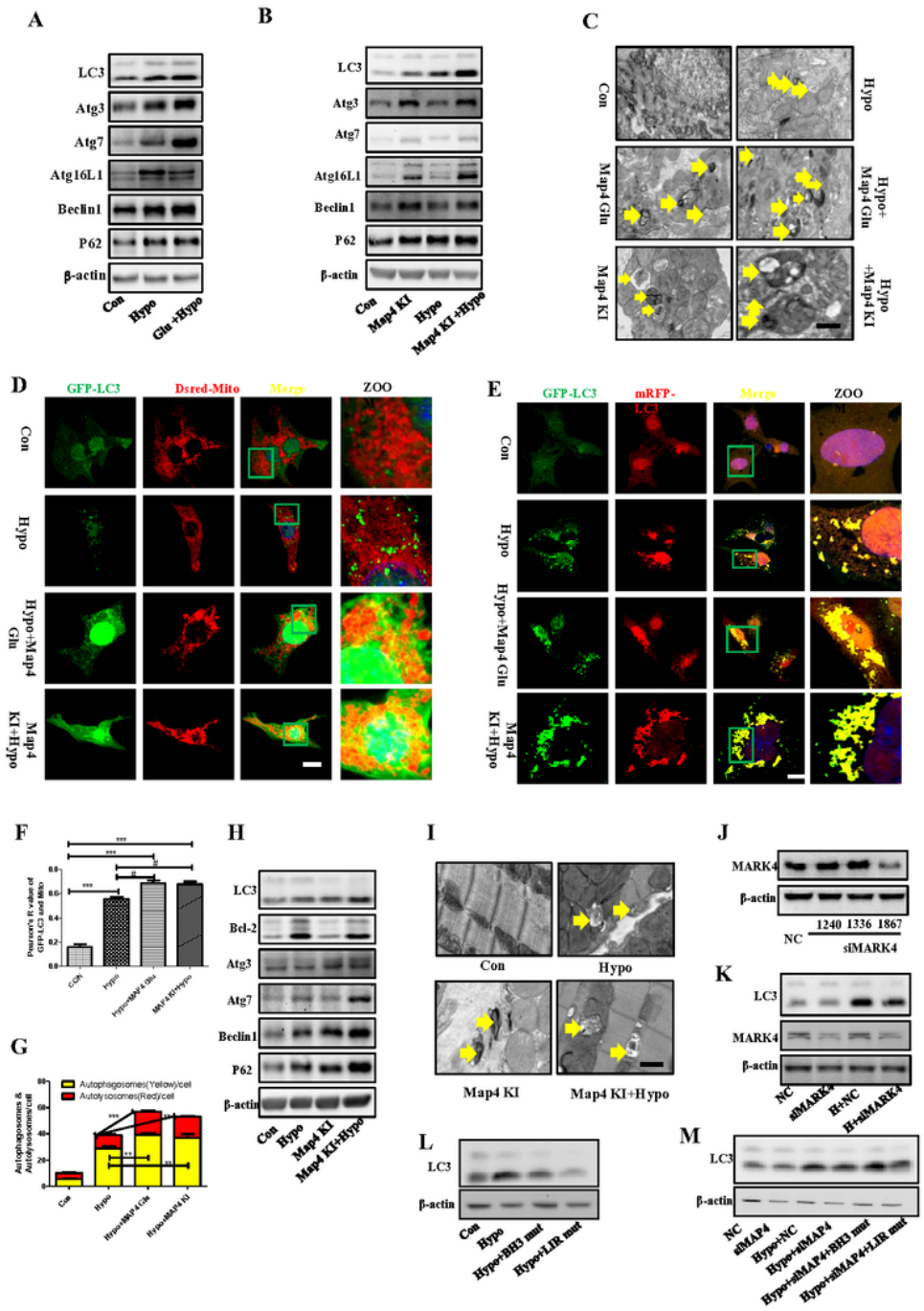

Figure 5

The MAP4 LIR (47–50aa) determinates p-MAP4 increased autophagy under hypoxic conditions. (A) Hypoxic cardiomyocyte specimens pre-treated with or without Ad-MAP4 (Glu) were collected to measure autophagy proteins, including LC3, Atg3, Atg7, Atg5-Atg12, Atg16L1, Beclin1, Bcl-2, and p62. n=5. (B) Representative images of mitophagy, detected by co-staining with GFP-LC3 and Dsred-Mito, in hypoxic primary cardiomyocytes pre-treated with or without Ad-MAP4 (Glu). Scale bar=10 μm. n=5. (C) The

mitophagosomes, measured by TEM, in cardiomyocytes after same treatment. Scale bar=0.5 μm. n=3. (D) Representative images of autophagic flux, measured by mRFP-GFP-LC3, in cardiomyocytes after same treatment. n=3. (E). Representative bands of autophagy proteins in hypoxic myocardium of wild-type and MAP4- KI mice. n=3. (F). Statistical analysis of Pearson's R value in (D). ***p<0.001 versus the Con group. #p<0.05 versus the hypoxic group. n = 3. (G) Statistical analysis of autophagosomes and autolysosomes in (F). **p<0.01 and ***p<0.001 versus the hypoxic group. n=3. (H). The MAP4-KI mice were exposed to hypoxia, and their specimens were used to detect autophagy-related proteins. n=3. (I). Representative images of mitophagosomes, detected by TEM, in MAP4-KI mice before or after hypoxia. Scale bar=0.5 μm. n=3. (J). Representative bands of MARK4 in cardiomyocytes. n=5. (K). Representative bands of MARK4 and LC3 in cardiomyocytes. n=5. (L) Representative bands of LC3 in primary cardiomyocytes treated by hypoxia with Ad-BH3 mutated MAP4 (Glu) and Ad-LIR mutated MAP4 (Glu). n=5. (M) Representative bands of LC3 in primary cardiomyocytes after specific treatment.

Supplementary Files

This is a list of supplementary files associated with this preprint. Click to download.

- Graphicabstract.pdf
- FigureS1.pdf